Check for updates

LIMNOLOGY and OCEANOGRAPHY: METHODS

ASLO

Limnol. Oceanogr.: Methods 19, 2021, 196–209
© 2021 The Authors. *Limnology and Oceanography: Methods* published by Wiley Periodicals LLC. on behalf of Association for the Sciences of Limnology and Oceanography.
doi: 10.1002/lom3.10414

Simultaneous recording of filtration and respiration in marine organisms in response to short-term environmental variability

Jahangir Vajedsamiei,[1]* **Frank Melzner**,[1] **Michael Raatz**,[2] **Rainer Kiko**,[1,3] **Maral Khosravi**,[1] **Christian Pansch**[1,4]

[1]Department of Marine Ecology, GEOMAR Helmholtz Centre for Ocean Research Kiel, Kiel, Germany
[2]Max-Planck Institute for Evolutionary Biology, Plön, Schleswig-Holstein, Germany
[3]Laboratoire d'Océanographie de Villefranche-sur-Mer, Sorbonne Université, Paris, France
[4]Department of Environmental & Marine Biology, Åbo Akademi University, Turku, Finland

Abstract

Climate change imposes unusual long-term trends in environmental conditions, plus some tremendous shifts in short-term environmental variability, exerting additional stress on marine ecosystems. This paper describes an empirical method that aims to improve our understanding of the performance of benthic filter feeders experiencing changes in environmental conditions, such as temperature, on time scales of minutes to hours, especially during daily cycles or extreme events such as marine heatwaves or hypoxic upwelling. We describe the Fluorometer and Oximeter equipped Flow-through Setup (FOFS), experimental design, and methodological protocols to evaluate the flood of data, enabling researchers to monitor important energy budget traits, including filtration and respiration of benthic filter-feeders in response to fine-tuned environmental variability. FOFS allows online recording of deviations in chlorophyll and dissolved oxygen concentrations induced by the study organism. Transparent data processing through Python scripts provides the possibility to adjust procedures to needs when working in different environmental contexts (e.g., temperature vs. pH, salinity, oxygen, biological cues) and with different filter-feeding species. We successfully demonstrate the functionality of the method through recording responses of Baltic Sea blue mussels (*Mytilus*) during one-day thermal cycles. This method practically provides a tool to help researchers exposing organisms to environmental variability for some weeks or months, to relate the observed long-term performance responses to short-term energy budget responses, and to explain their findings with the potential to generalize patterns. The method, therefore, allows a more detailed description of stress-response relationships and the detection of species' tolerance limits.

Benthic filter-feeders play critical roles in the cycling of nutrients and energy in numerous marine habitats (Gili and Coma 1998; Dame et al. 2001). Their filtration activity can regulate the load of suspended particulate organic matter and contaminants such as heavy metals (Widdows et al. 1998) as well as the population density and community structure of microplanktonic primary producers and pathogens in shallow waters (Burge et al. 2016). Due to their profound effect on structural heterogeneity, species diversity and functioning of ecosystems, various species of benthic filter-feeders are viewed as ecosystem engineers (Dame et al. 2001). Besides, benthic filter-feeders support commercially important aquaculture industries that provide food and non-food services with an annual global worth of ~ 35 billion US dollars (van der Schatte Olivier et al. 2018).

In shallow marine ecosystems, benthic filter-feeders can experience short-term systematic or stochastic fluctuations in ambient seawater conditions (daily to weekly cycles) due to weather events, irradiance variation, tides or wind-driven changes in water levels, upwelling and downwelling events, and changes in biological activity (Boyd et al. 2016; Wahl et al. 2016). Ongoing climate change induces long-term (annual to decadal) unusual trends in environmental conditions (e.g., warming, acidification, and deoxygenation), as well as shifts in short-term fluctuation patterns of environmental regimes (Lima and Wethey 2012), which threatens benthic taxa, including filter-feeders (Przeslawski et al. 2008). To advance our empirical understanding of organisms' performance in a changing ocean, developing experimental setups for high-temporal resolution monitoring of organisms' energetics traits in dynamic environments and automated data processing is crucial. This enables a more detailed description

*Correspondence: jvajedsamiei@geomar.de

Additional Supporting Information may be found in the online version of this article.

This is an open access article under the terms of the Creative Commons Attribution License, which permits use, distribution and reproduction in any medium, provided the original work is properly cited.

of stress-response relationships and detection of species' tolerance limits.

The two most important energy budget traits of benthic filter-feeders, filtration (feeding), and respiration rates can be monitored through flow-through setups (Riisgård 2001; Filgueira et al. 2006; Bayne 2017). In a closed chamber setup (including intermittent closure techniques), the filtration activity of the organism can substantially decrease or stop due to depletion of food before a significant oxygen-depletion signal (i.e., respiration) can be detected (Widdows 1976) and the physicochemical conditions can be controlled less efficiently. Importantly, during exposure to suboptimal food levels, filter-feeders usually decrease and decelerate their filtration and aerobic metabolism to conserve energy (Kittner and Riisgård 2005; Riisgård et al. 2006; Tang and Riisgård 2016). In a flow-through setup, the experimental food level can be manually or automatically maintained within the range of interest. However, so far, the application of flow-through setups has been mostly limited to investigations on a single response (filtration or respiration) to constant treatment conditions (Riisgård 2001; Filgueira et al. 2006; Pleissner et al. 2013). Widdows (1973) measured filtration or respiration of mussels under constant temperatures based on weekly snapshot-measurements of phytoplanktonic food and dissolved oxygen concentrations in water flowing into and out of an experimental chamber using an oximeter and a Coulter counter. High-temporal resolution (continuous) recording of filtration and respiration responses in parallel was only described by Haure et al. (2003) who used a flow-through setup equipped with a laboratory fluorometer and an oximeter in a short (3 h) experiment. One limiting factor preventing more frequent use of such experimental setups in the past could have been the high cost of measurement equipment (especially the laboratory fluorometer) limiting replication of measurements. Furthermore, it is technically challenging to record the responses of filter-feeders exposed to environmental fluctuations in an air- and water-tight flow-through setup, as time, temperature, and other physical and chemical factors can confound measurements.

In this paper, we present an experimental method developed for monitoring rates of filtration and respiration in parallel as well as simplistic estimation of filter-feeders' surplus of energy available for growth (scope for growth [SFG]), in response to short-term environmental fluctuations. We describe the design of our setup in conjunction with the protocols used for semiautomated data processing. We also implement and test the method in an experiment on the responses of blue mussels (*Mytilus* spp.) from the Baltic Sea to daily thermal fluctuation cycles. Finally, we discuss the benefits and constraints of the setup and recommend directions for future applications, such as its potential applicability to multifactorial investigations.

Use materials and procedures

The setup

We designed a Fluorometer- and Oximeter-equipped Flow-through Setup (FOFS) with the ability to simulate thermal regimes and to record physiological parameters of benthic filter-feeders. FOFS is schematically illustrated in Fig. 1 (see also the photographic view in Supplementary Information Fig. S1). The peristaltic pump "Pump1" (ISMATEC MCP 12 channels, Cole-Parmer) creates a constant flow of seawater from a multi-parameter-controlled source tank (600 L; Kiel Indoor Benthocosms, KIBs, described in Pansch and Hiebenthal 2019) to the "dilution tank" (250 mL). The peristaltic pump "Pump2" (ISMATEC REGLO digital four channels, Cole-Parmer) produces a steady flow of phytoplankton food suspension from the "food tank" to the dilution tank. The cryptophyte *Rhodomonas salina* (cultured at 16°C by the Kiel Marine Organism Culture Centre at GEOMAR, KIMOCC) is applied as the food source in our setup as in many other experiments with filter-feeding marine invertebrates (Clausen and Riisgård 1996; Riisgård et al. 2013; Sanders et al. 2018). Before each experiment, the food tank ($\sim$ 10 liters) is filled with a high-concentration *R. salina* suspension (e.g., $\sim 3 \times 10^5$ cells mL^{-1}). The food concentration in the dilution tank can be adjusted according to the needs of the study organisms by varying concentration, composition, and pumping rates of Pump1 and Pump2. The resulting food suspension is pumped from the dilution tank into four separate paths ($Path_C$ and $Path_{S1–3}$). $Path_C$ represents the control path where oximetry and fluorometry are conducted in the absence of the study specimen, while $Path_{S1–3}$ can harbor one or more specimen per unit (Fig. 1; Fig. S1). For higher replication, the number of parallel paths can be easily increased. Along each path, the food suspension flows first into a cylindrical Plexiglas chamber (100 mL; incubation or oximetry chamber) through an inlet at its lower part of the sidewall. After filling the chamber, the suspension flows out via an outlet at the top of the incubation chamber and into a cylindrical nontransparent PVC chamber (350 mL; fluorometry chamber). Finally, the suspension discharges from the outlet located at the upper part of the fluorometry chambers. Relatively thin (here 0.80- and 2.54-mm inner diameter in Pump2- and Pump1-paths, respectively) silicon tubes in the setup reduce settling rates of the phytoplankton suspension. Plexiglas tube-compatible connectors are used as inlets and outlets of the chambers. The suspensions inside the food and dilution tanks, and incubation and fluorometry chambers are steadily mixed by laboratory magnetic stirrers (HI190M, HANNA instruments; Fig. 1a,b; Fig. S1).

Dissolved oxygen concentration is recorded via sensor spots (SP-PSt3-NAU, PreSens Precision Sensing; resolution ± 0.1% O_2 at 20.9% O_2 or ± 0.04 mg L^{-1} at 9.1 mg L^{-1}) attached to the inner surface of the incubation chambers (Fig. 1a,b; Fig. S1). Sensor spots are read out by an oximeter (OXY-4 mini, PreSens Precision Sensing) through optical fibers connected to the cylinders' outer surface. Configuration and data logging are achieved using the corresponding software. Sensor spots are calibrated based on the two-point calibration protocol (PreSens 2017). The reference measurements were conducted in anoxic water (prepared by dissolving 10 g of sodium sulfite in 1000 mL water) and water-vapor saturated air.

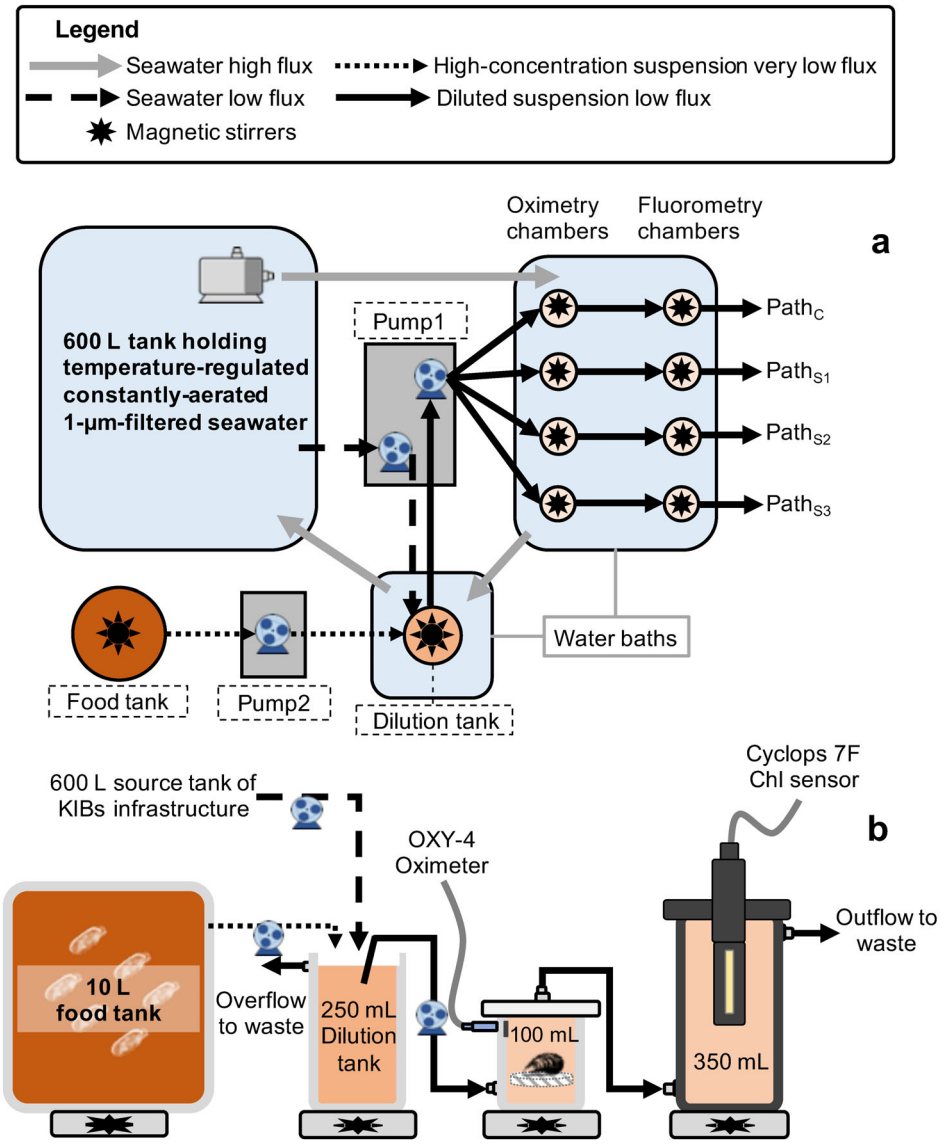

Fig. 1. Schematics of the Fluorometer- and Oximeter-Equipped Flow-through Setup (FOFS). (**a**) Schematic top view indicating the flux of seawater, concentrated and diluted food suspension (depicted by the brown shading) through the setups' main components, including the source-water tank, the food tank, the dilution tank, water baths, and incubation (Plexiglas, 100 mL) and fluorometry (PVC, 350 mL) chambers. $Path_C$ indicates the control path where oximetry and fluorometry are conducted without any study specimen. During a trial, filter-feeders are placed within the incubation chambers ($Path_{S1–3}$). (**b**) Schematic side view indicating the flux of suspension in $Path_{Sn}$. The dissolved oxygen and chlorophyll concentrations are recorded within the incubation (oximetry) and fluorometry chambers, respectively.

Food concentration is measured using fluorometers (Cyclops 7f, Turner Designs; application: chlorophyll in vivo, blue excitation; minimum detection limit: 0.00003 mg L^{-1}; linear range: 0–0.5 mg L^{-1}) in dark and well-mixed conditions inside the fluorometry chambers (Fig. 1; Fig. S1). Fluorometers are set up and data are recorded using the Cyclops-explorer connectors and software (Turner Designs).

The size of incubation (oximetry) chambers must be large enough to satisfy the space requirements for the species' normal activities (i.e., related to the size of study specimens). The volume of the fluorometry chamber is chosen to provide a distance of ~ 8 cm between the fluorometer's optical face and the chamber floor while the optical face and shade caps of the fluorometer are entirely submerged (Turner Designs 2020).

The source-water tank (600 liters) is equipped with a control system (Profilux 3.1TeX; GHL Advanced Technology) automating thermal simulations. A temperature profile (in .csv format) is submitted via the GHL-controller software to the ProfiLux computer, which then adjusts the source-water temperature. More parameters (pH/pCO_2, salinity, etc.) can also be manipulated in automated procedures. This type of GHL-equipped source-water tank has been successfully implemented within

the Kiel Indoor and Outdoor Benthocosm systems (for more details, *see* Wahl et al. 2015 and Pansch and Hiebenthal 2019).

To minimize heat loss in FOFS, a water pump (EHEIM) generates a flux of source water (~ 2 L min^{-1}) into two water baths positioned in sequence: the first water bath (aquarium of $50 \times 30 \times 15$ cm) holds incubation and fluorometry chambers and the second water bath ($20 \times 15 \times 10$ cm) holds the dilution tank (Fig. 1a). Additionally, air-exposed areas of silicon tubes are covered by heat-reflective thermal blankets to conserve heat.

If the source water becomes supersaturated with air, the formation of air bubbles can disturb the oximetry and fluorometry. This can be avoided by intensive aeration of the source-tank water during the experiment.

General experimental design and procedure

A randomized block design can be used for experimenting with FOFS. Each experiment can involve several temporally repeated trials with similar treatments but different study specimens. Each trial has three subsequent stages, a pre-, a main-, and a post-trial (for an exemplary scheme, *see* Fig. 2). During pre- and post-trials, the setup runs in the absence of specimens for ~ 3 h at a constant baseline temperature until the readout of all sensors becomes and remains stable for > 60 min (Fig. 2). Later in the data processing, we use data of each pre- and post-trial to account for the baseline dissimilarities between readouts of different sensors and to check whether measurements were affected by random factors over the corresponding main trial.

During all stages of a trial, one of the paths (i.e., $Path_C$) acts as the control. Accordingly, the incubation chamber located on $Path_C$ contains only the temperature logger (EnvLogger, ElectricBlue) but no filter-feeder. After the pre-trial, the other incubation chambers located on $Path_{Sn}$ are de-capped, and the study specimens are placed on plastic-mesh seats inside the chambers (Fig. 1b). The chambers are then recapped, avoiding air bubbles. At this point, the fluorometry chamber caps must be also repositioned to eliminate potentially trapped air bubbles.

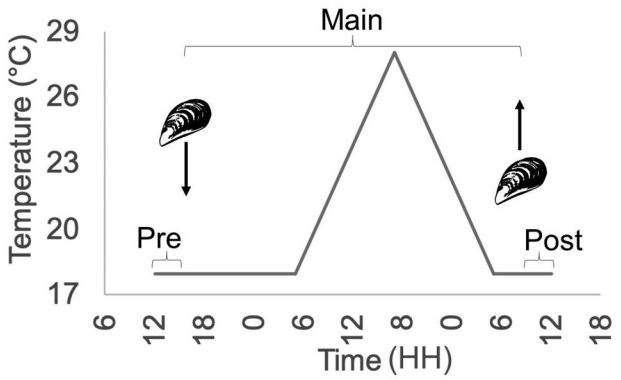

Fig. 2. An exemplary trial with a daily thermal fluctuation cycle is indicated. The main trial is preceded and followed by a pre- and post-trial period without filter-feeder, respectively. During the main trial, the organisms' response to fluctuation is recorded. The main trial can also comprise periods of a constant condition before and after the fluctuation, which allows organisms to acclimate to the ambient condition and provides insight into how consistent the responses are during exposure to a static ambient condition.

After each post-trial, and before starting a new pre-trial, FOFS must be run with deionized water for ~ 20 min and the chambers' interior must be brushed thoroughly to remove remnants of the studied specimens (e.g., feces and associated microbial biota).

Data processing through python scripts

Here, an overview of different steps of the data processing is provided with a focus on the techniques used to correct and convert measurements and calculate the response variables. The associated Python scripts can be found in the Supplementary Information Scripts. Notes and explanatory remarks provided throughout the scripts clarify how the steps and commands in the scripts work and how one can use and adopt them.

Dissolved-oxygen concentration calculator

"DO_calculator.py" (Supplementary Information Script S1) transforms the phase angle data (phi) collected via PreSens Pts3 sensor spots (and Oxi4-mini oximeter) to the dissolved-oxygen concentration in % air-saturation considering the temperature-sensitivity of the phase angle and Stern–Volmer constant. The % air-saturation data are then converted to μmolO_2 L^{-1} considering ambient temperature and salinity. The ambient temperature data used in the processing are recorded by the logger placed within FOFS. The equations used in this calculator are based on the Oxi4-mini instruction manual (PreSens 2004).

Future users applying oximeters lacking the automatic temperature-correction and unit conversion can revise the script based on the specifications of their device (sensors).

Trial-by-trial analysis

"FOFS_trial-by-trial_processing.py" (Supplementary Information Script S2) can be applied to process raw data and generate outputs including data frames and time series plots of raw, corrected, and converted versions of measurements and calculated data of the response variables for each experimental trial.

Step 1 (filtration and feeding rates)

The script reads in pre-trial series of food concentration (mV) and names them "pre_C_mV_Chl" or "pre_Sn_mV_Chl." The series are denoised (trended) using a time-windowed slider with an iterative robust location estimator such as Tukey's biweight or Welsch estimators (Wotan module; Hippke et al. 2019). Robust estimation assigns more weight to the data points closer to the central values of the sliding window (for a detailed description of different types of estimators, refer to Hippke et al. 2019). The trended mV series suffixed by "_Trend" are then corrected using the temperature correction coefficient (Supporting Information Text S1) and saved with the additional suffix "_TC."

The trended- and temperature-corrected mV series are plotted to select the "pre-trial stable-data." The criterion for selecting the stable-data is explained in Supplementary Information Text S2. The pre-trial stable-data of $Path_C$ is averaged and then converted from mV to cells mL^{-1} using the conversion coefficient (Supporting Information Text S1), which will be used later as "the initial concentration." Ideally, the conversion coefficient is checked at each pre-trial since it might change slightly due to variation in the positioning of the fluorometer on the chamber and the rate of magnetic stirring.

The main trial mV series are also denoised and, then, corrected using the temperature-correction coefficient (Fig. 3b). The mV data of each sensor are then expressed as percentage of the mean value of the pre-trial stable-data of the same sensor (named "percent_C" and "percent_Sn" in the script). This procedure eliminates the baseline differences in the absolute value of output between the fluorometers as the output of each fluorometer is directly proportional to the chlorophyll (*R. salina*) concentration signal (Cyclops 7 User's Manual; $R^2 > 0.985$ based on our observations). The food concentration series are finally converted from the percentage to cells mL^{-1} ("cell_per_ml_C" and "cell_per_ml_Sn"), considering that the "initial cell concentration" is 100% (compare Fig. 3b with Fig. 3c).

In each FOFS path, the fluorometry chamber, which has a 350-mL volume due to the space requirements of the fluorometer (refer to Use material and procedures: The setup), is inevitably positioned downstream to the incubation (oximetry) chambers (Fig. 1b). The oximetry chamber contains a relatively small volume of a well-mixed solution. Any change in the respiration or filtration activities of the study specimen almost instantly alters the dissolved oxygen or food concentration in the oximetry chamber and in the inflow to the fluorometry chamber. The inflow is being mixed with the solution in the larger fluorometry chamber; therefore, any measured change in food concentration is a dampened (temporally lagged and weakened) version of a change in the inflow food concentration. The script uses a linear differential equation (Campbell and Haberman 2008; Supporting Information Text S3) to improve the estimation of rapid changes in the measured food concentration (Fig. 3c,d). These rapid changes in food concentration can occur because of filtration shutdown or recovery of the study organism. Notably, if the measured food concentration follows a consistent trend with no rapid changes, no correction is done (Supplementary Information Fig. S3).

The resulting time-series is used to calculate the filtration and feeding rates of study specimens (Fig. 3e) based on Eqs. 1 and 2, respectively (modified after Larsen and Riisgård 2011).

$$\mathrm{filt_{Sn}}\left(\mathrm{mL\,min^{-1}}\right) = \frac{\mathrm{food_C}\left(\mathrm{cells\,mL^{-1}}\right) - \mathrm{food_{Sn}}\left(\mathrm{cells\,mL^{-1}}\right)}{\mathrm{food_{Sn}}\left(\mathrm{cells\,mL^{-1}}\right)} \times \mathrm{flow\ rate}\left(\mathrm{mL\,min^{-1}}\right) \quad (1)$$

$$\mathrm{feed_{Sn}}\left(\mathrm{cells\,min^{-1}}\right) = \mathrm{food_C}\left(\mathrm{cells\,mL^{-1}}\right) - \mathrm{food_{Sn}}\left(\mathrm{cells\,mL^{-1}}\right) \times \mathrm{flow\ rate}\left(\mathrm{mL\,min^{-1}}\right) \quad (2)$$

The final time series of filtration and feeding rates are named "filt_ml_per_min_Sn" and "feed_cell_per_min_Sn" in the script.

Step 2 (respiration rate)

The same techniques are used to denoise pre- and main-trial dissolved oxygen concentration (% air-saturation and μmol L^{-1}) and to define and average the "pre-trial stable-data" (refer to Step 1; Fig. 4a,b).

There might be small baseline differences between the outputs of the oximeters due to imperfect sensor calibration. For example, we calibrated the sensor spots twice manually and twice using the calibration data provided in the Final Inspection Protocol for the PreSens Pts3 sensor spots. The differences between the sensors when FOFS was running in the absence of filter-feeders were comparable to the differences recorded in air (i.e., < 1.2% air saturation). The sensors' baseline outputs may be even more comparable if the sensors are calibrated in a shared calibration medium, although this is hard to conduct when the sensor spots are attached to different chambers. Nonetheless, the average pre-trial stable measurement of each $sensor_{Sn}$ is subtracted from the counterpart value of the $sensor_C$, and this baseline difference is later added to the main-trial data of the $sensor_{Sn}$ (Fig. 4c). Notably, this correction simplistically assumes that the calibration curves of $sensor_{Sn}$ and $sensor_C$ are nearly parallel over the experimental range of dissolved-oxygen concentration and therefore imposes cumulative errors as the measured concentration of $sensor_{Sn}$ deviate from the pre-trial reference. For example, if the difference between measurements of $sensor_{S1}$ and $sensor_C$ is $\sim 1\%$ at a real ambient concentration of 100% air saturation, after the correction the two values will depart < 0.1% per 10% decrease in the ambient concentration.

The final version of main-trial data (named "control_ymol_per_l_C" and "corrected_ymol_per_l_Sn" in the script) are then applied to Eq. 3 to calculate the respiration rate.

$$\mathrm{resp_{Sn}}\left(\mu\mathrm{molO_2\,min^{-1}}\right) = \left(\mathrm{oxyg_C}\left(\mu\mathrm{mol\,L^{-1}}\right) - \mathrm{oxyg_{Sn}}\left(\mu\mathrm{mol\,L^{-1}}\right)\right) \times \mathrm{flow\ rate}\left(\mathrm{L\,min^{-1}}\right) \quad (3)$$

Step 3 (scope for growth)

The principal outputs of data processing are filtration and respiration records. The script also provides a very simplistic estimation of surplus of energy available for growth based on the assimilated energy minus the respired energy (the basic definition of the SFG; Widdows 1976). The SFG can be estimated based on the experimental feeding rate (Eq. 4) or, instead, based on the feeding rate at a hypothetical food

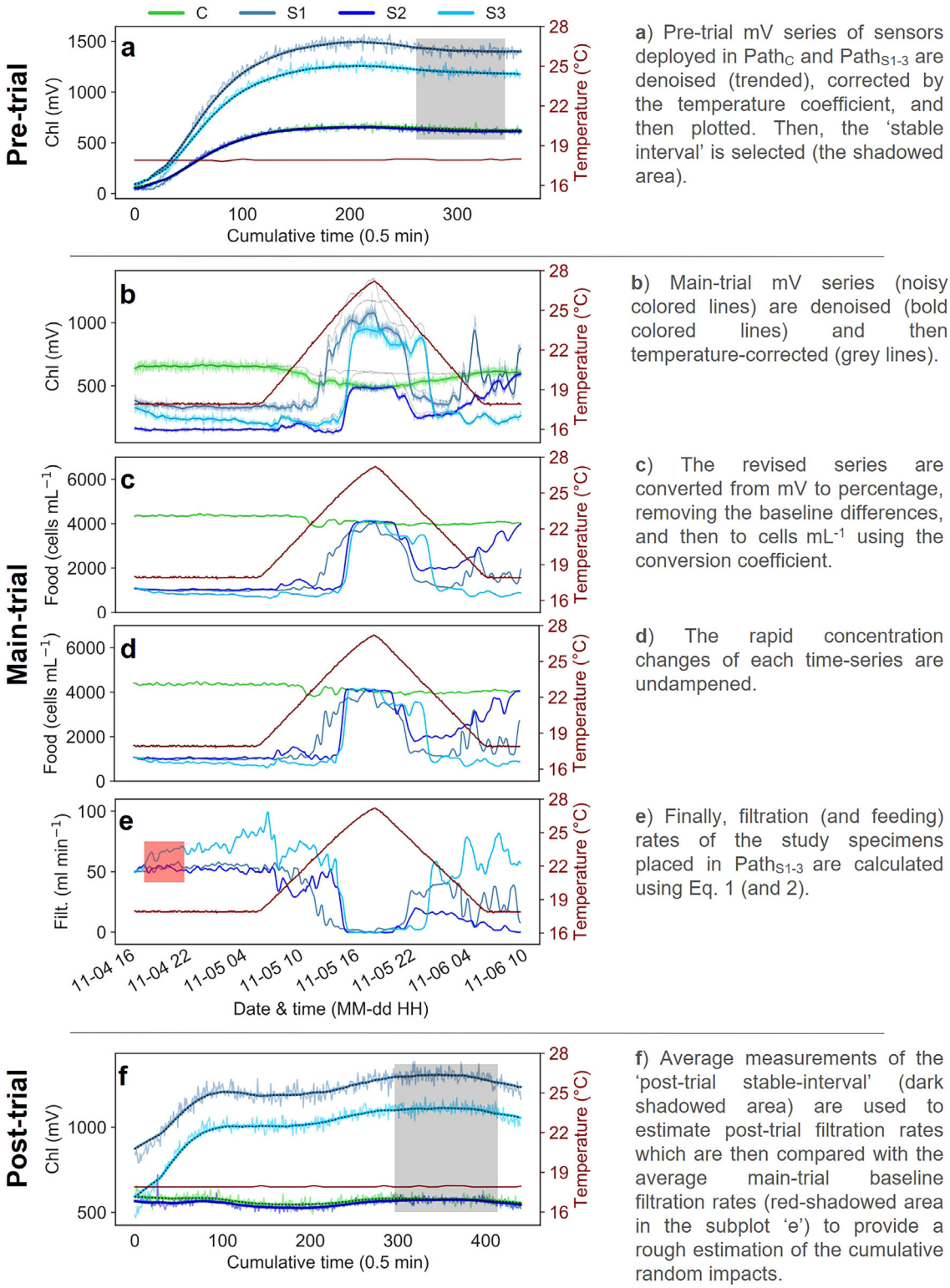

Fig. 3. Data processing flowchart with acquired time-series graphs of fluorescence intensity in mV, *Rhodomonas salina* concentration, and mussel (*Mytilus* spp.) filtration rates for an experimental trial (04–06 November 2019) including pre- (**a**), main- (**b**–**e**), and post-trial (**f**) stages. Data from Path$_C$ (the control path) are displayed as green lines. Data from Path$_{S1-3}$ are displayed as shades of blue (see the legend at the top of the plot). The measurement frequency is 0.5 min (x-axis titles of pre- and post-trial subplots).

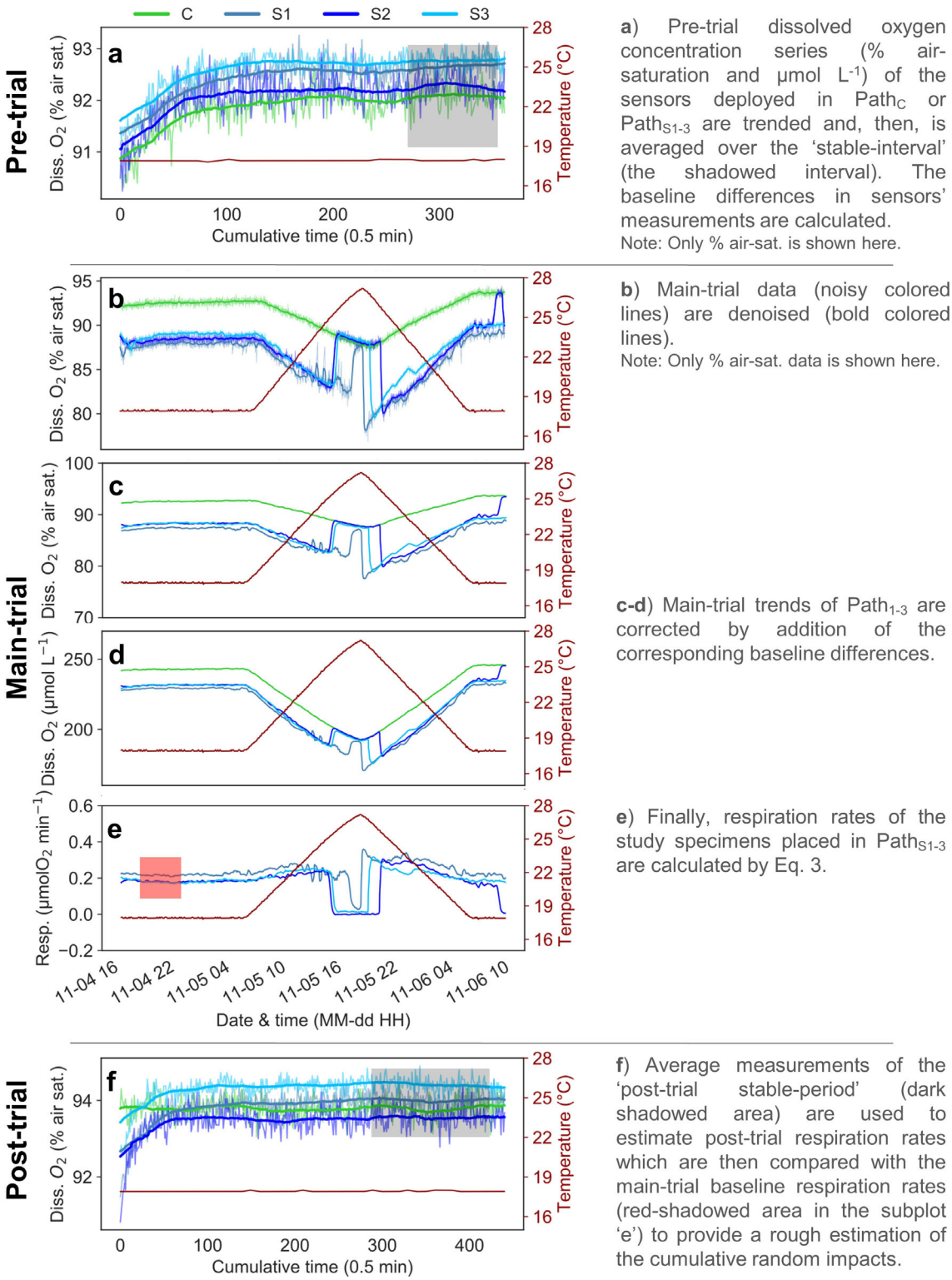

Fig. 4. Data analysis flowchart with acquired time series graphs of the dissolved-oxygen concentration and mussel (*Mytilus* spp.) respiration rates for an experimental trial (04–06 November 2019) including pre- (**a**), main- (**b**–**e**), and post-trial (**f**) stages. The measurement frequency is 0.5 min (x-axis titles of pre- and post-trial subplots).

concentration (e.g., the average experimental food concentration). The hypothetical feeding rate ($feed_{hypSn}$ in J h^{-1}) is calculated based on the filtration rate at a constant food concentration $food_{hyp}$ in J mL^{-1} (Eq. 5). SFG_{hypSn} is then estimated based on $feed_{hypSn}$, $resp_{Sn}$ (i.e., the respiration rate in J h^{-1}), and the assimilation efficiency (AE) of 80% (based on the average value reported in Widdows and Bayne 1971) through Eq. 6.

$$SFG_{Sn}\left(J\,h^{-1}\right) = feed_{Sn}\left(J\,h^{-1}\right) \times AE - resp_{Sn}\left(J\,h^{-1}\right) \quad (4)$$

$$feed_{hypSn}\left(J\,min^{-1}\right) = filt_{Sn}\left(mL\,min^{-1}\right) \times food_{hyp}\left(J\,mL^{-1}\right) \quad (5)$$

$$SFG_{hypSn}\left(J\,h^{-1}\right) = feed_{hypSn}\left(J\,h^{-1}\right) \times AE - resp_{Sn}\left(J\,h^{-1}\right) \quad (6)$$

Conversion factors of 1.75 μJ per *R. salina* cell (Kiørboe et al. 1985) and 450 kJ per $molO_2$ (Widdows and Hawkins 1989) are applied.

Step 4 (cumulative random effects)

FOFS assumes that the deviations in food and dissolved-oxygen concentrations between $Path_C$ and each $Path_{Sn}$ are only due to the study specimens' filtration and respiration during the main trial. Therefore, it is important to check the possible contribution of random (non–filter-feeder) factors. To do so, the average of the "post-trial stable-data" (of each $sensor_{Sn}$) is used to assess how close the post-trial filtration and respiration rates are to zero (refer to Figs. 3f, 4f). Post-trial responses are expected to be equal or close to zero, as this stage is conducted in the absence of study specimens. The post-trial responses are compared with the main-trial baseline filtration and respiration rates to roughly estimate the ratios of the non–filter-feeder- to filter-feeder-induced signals (i.e., the cumulative random impacts in percent; refer to Figs. 3e,f, 4e, f). Baseline filtration or respiration rate is defined in the script as the average of 180th to 480th main-trial data points, while future users may need to change the interval based on the observed responses.

It must be considered that cumulative random effects are those non–filter-feeder (confounding) effects which are still detectable after the main trial (in the post-trial stable-data), which could be due to long-lasting drifts in sensor measurements, bacterial respiration which may be boosted due to remnants of the study specimens (i.e., ammonia/feces released), settlement of the food-organism (in this case *R. salina*) and possible changes in the speed of magnetic stirrers. Future users need to also ensure that their measurements are not impacted by transient random effects (e.g., temporary electrical interventions and sensor malfunctions) through "blank trials" (for an example, *see* Assessment and discussion: Demonstration experiment).

FOFS integrative processing

The data frames created through the trial-by-trial processing can be integrated using "FOFS_integrative_processing.py" (Supplementary Information Script S3). Importantly, a data sheet containing dry weights and shell lengths of study specimens (e.g., Supplementary Information Table S1) must be manually added to the experimental folder, before executing the script.

The script first merges post-stage data frames, including all estimated cumulative random effects ("%_cumulative_random_effects_Sn" in the script). Then, it concatenates main-trial data frames one by one, plus defining size-standardized rates of filtration, feeding, respiration, and SFG for the replicates. All responses are standardized to shell length and dry tissue weight as proxies for gill surface area and tissue volume (Hamburger et al. 1983; Riisgård 2001). Any change to the complete experimental data frame ("experiment_df"), such as excluding a broken part, can be done through "manual imposition of changes."

The script produces line plots, each aggregating over replicated values of a specific variable at each time point and shows estimates of the averages with the respective 95% confidence intervals.

Finally, thermal variations in responses are described through Generalized Additive Models (pyGAM module; Servén and Brummitt 2018) using data of the whole experiment or a specific phase of it (e.g., the warming or cooling phase of a thermal fluctuation treatment). The best fit GAM is selected using a grid search over multiple values of the regularization parameter and n-spline values seeking the lowest Generalized Cross-Validation score (for more details on GAM, refer to Wood 2017).

Assessment and discussion

Demonstration experiment

In a few studies, flow-through setups were applied for simultaneous measurement of filtration and respiration of aquatic organisms under static experimental conditions (Widdows 1973; Haure et al. 2003). Besides, guidelines are available for the design of flow-through setups proper for measuring the filtration rate under static conditions (Filgueira et al. 2006; Larsen and Riisgård. 2011). Here, we describe the design of a FOFS and provide the protocols used for semiautomated data processing through Python scripts. The method described here allows for high-resolution monitoring of filtration and respiration rates in response to dynamic environmental conditions, ultimately enabling the detection of the ecological limits of benthic filter feeders facing climate change. The methods' functionality is tested in a demonstration experiment, testing the key assumption that the deviations of processed concentrations of each specimen path ($Path_{Sn}$) from those of the control path ($Path_C$) of FOFS in time is only due to the respective filter-feeder being examined during a dynamic treatment.

In many shallow-water marine habitats (including the Baltic Sea), temperature changes at time scales of seconds, minutes or hours to days and weeks, during daily temperature

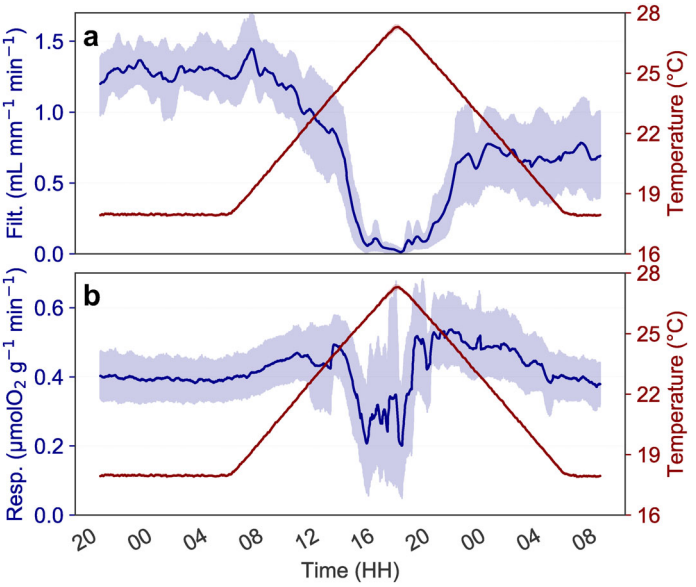

Fig. 5. Temporal variation in the length-specific filtration rate (**a**) and weight-specific respiration rate (**b**), along the daily temperature cycle. Data were pooled over multiple trials and replicates (10 replicates blocked in time) in the demonstration experiment. Replicated values were averaged at each time point, presented with 95% confidence intervals.

cycles, heatwaves and/or upwelling events (Lima and Wethey 2012; supplementary information in Pansch and Hiebenthal 2019). Therefore, we applied our newly developed method in six trials using daily thermal cycles.

In four trials, we exposed mussels (*Mytilus* spp. specimens from Kiel Fjord, Western Baltic Sea) to daily temperature fluctuations. Before the trials, study specimens were kept at constant 16°C and fed once per day with *R. salina* for 3 weeks. The minimum and maximum temperatures experienced by the mussels in the main trials were 18°C and 27.5°C, which were reached at 5:00 and 17:00 during the day, respectively. The rate of linear change (rise and decline) was ± 0.79°C h^{-1}. After each trial, all specimens were kept in 0.5 μm filtered seawater at room temperature (16°C) for ~ 10 h to release feces (minimizing the effect of feces-weight on mussel dry tissue weight). Afterward, the length of specimens was measured using a caliper and their tissue was dried at 80°C for 30 h and weighed using an electronic balance (0.1 mg; Sartorius). Besides, we checked that the thermal exposures do not impose substantial changes on the phytoplanktonic food (*Rhodomonas salina*) concentration (Supplementary Information Text S4 and Fig. S4).

Two blank trials, each with a pre- and a main-trial phase, were conducted to check whether processed measurements of different sensors remain comparable over the experimental time and over the temperature range in the absence of mussels. The prestage of the first blank trial (14–16 October 2019) was carried out following the standard cleaning procedure. The prestage of the second trial (01–03 November 2019) was initiated as a follow-up of the mussel-inclusive trial (without the cleaning) to see how remnants of the mussels (e.g., ammonia/feces released, which might have possibly affected microbial activities in the tubing and chambers) could have affected the respiration and filtration time series under the influence of temperature and time over the main trial. The minimum and maximum temperatures in our two blank trials were 18°C or 20°C and 28°C or 29°C, respectively.

During all demonstration trials, seawater salinity was ca. 21 PSU, and the flow rates of Pump1 and Pump2 were constantly 16 and ~ 2 mL min^{-1}, respectively. The food tank was refilled with concentrated food-solution after each trial. The sensitivity of the fluorometers was set to X10, which is suitable for measuring in the range of 1 to 5 μg Chl L^{-1}, comprising the concentration range of our experiment. Readout frequencies of the fluorometers, the oximeter, and the temperature logger were set to 30 s.

All data of the demonstration experiment, including blank and mussel trials' data, are archived and accessible in Pangaea (www.pangaea.de; Vajedsamiei et al. 2020).

Blank trials provide a performance check

Trends of food or dissolved oxygen concentration were comparable between Path$_{Sn}$ and Path$_C$ over the main stage of the blank trials, supporting the main assumption that differences between Path$_{Sn}$ and Path$_C$ should only emerge from the study specimens (Supplementary Information Fig. S5). There were minor temporal decreases in food concentration (Supplementary Information Fig. S5a,c), possibly due to settlement and/or death of *R. salina* cells. As both, oxygen solubility in seawater and the rate of dissolved-oxygen removal within the FOFS tubing and chambers are temperature-dependent, oxygen content varied linearly with temperature (Supplementary Information Fig. S5b,d). Due to the constant air bubbling of the source tank, the source water remained saturated (~ 100%) with oxygen (confirmed by a WTW dissolved oxygen concentration meter, Multi 3630 IDS).

Calculated filtration and respiration rates stayed consistently close to zero with slight variability for both blank trials (Supplementary Information Fig. S6). The mean and standard deviation of responses during the main stage of the two blank trials are reported in Supplementary Information Table S2.

The prestage of the second blank trial ("01_nov") was done as an immediate follow-up of a mussel-trial, without cleaning of the system. Its outcomes indicate that remnants of the mussels did not cause notable deviations in concentration between Path$_C$ and each Path$_{S1–3}$ under the influence of temperature and time over the main trial. In the second blank trial, slight (transient) irregularity in dissolved-oxygen records of Path$_C$ caused minor transient drifts in the calculated respiration rates of Path$_{S1–3}$ (Supplementary Information Figs. S5d, S6d), contributing almost half of the mean respiration rate (Supplementary Information Table S2). Random transient irregularities were also observed in chlorophyll data but affected data of all four paths similarly. Yet, these random drifts

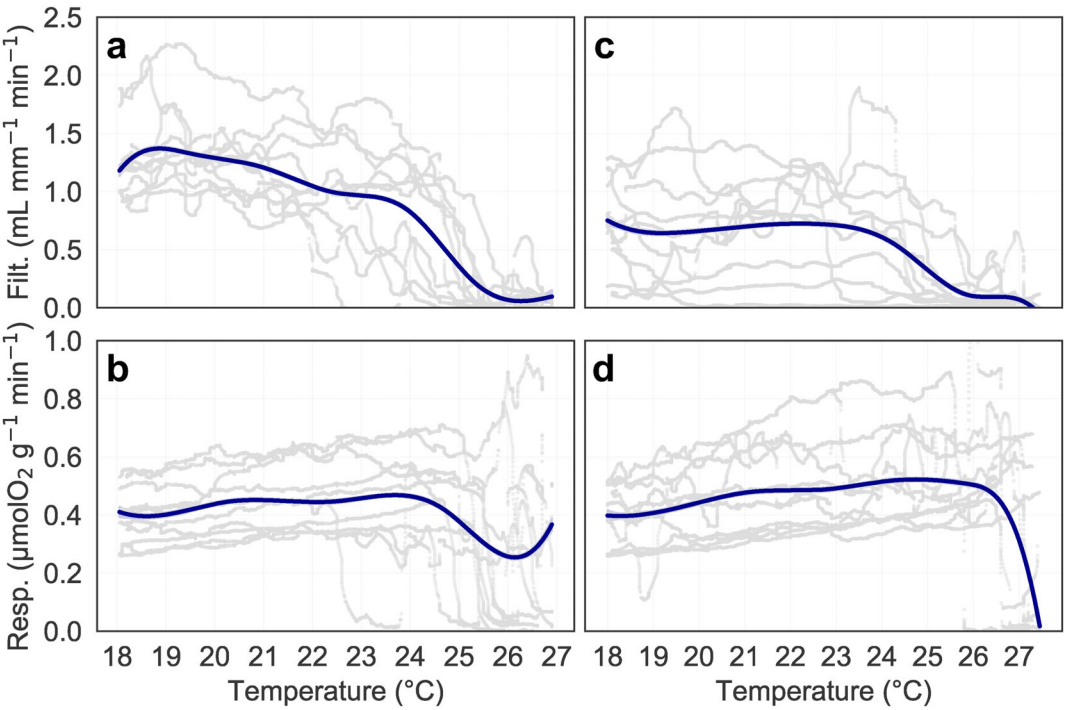

Fig. 6. Thermal response curves. Filtration and respiration rates of mussels as functions of the temperature in the warming (**a**,**b**) and cooling phases (**c**,**d**) of the mussel trials of demonstration experiment, modeled by the best-fit generalized additive models (dark-blue lines). The warming and cooling phases correspond to the time intervals 5:00–17:00 and 17:00–5:00, respectively.

are minor compared to the filter-feeders' response signal (compare Supplementary Information Fig. S5 with Fig. 5). Random irregularities might be explained by voltage fluctuations during working hours when high loads of electricity are being used. Future users may need to apply an online Uninterruptible Power Supply (UPS) to stabilize the voltage.

Mussel trials confirm applicability

The mussels induced differences in food and dissolved oxygen concentrations between $Path_{S1–S3}$ and the control ($Path_C$), which were used to define filtration and respiration rates (Supplementary Information Figs. S7, S8). In one mussel trial, the specimen of $Path_{S3}$ expressed filtration shutdown and intermittent respiration shutdowns before being exposed to the thermal fluctuation, which was different from the responses of other studied mussels (Supplementary Information Fig. S8c,d). Besides, in another mussel-trial, the resumption of respiration of the specimen of $Path_{S2}$ resulted in unusually high respiration rates (Supplementary Information Fig. S8f), due to magnetic stirrer arrest preventing efficient mixing of the solution inside the oximetry chamber. As the size of the studied mussels was large, the release of hypoxic water trapped within the shells during the metabolic depression resulted in a decrease in oxygen concentration recorded when the medium was not mixed efficiently. Data of these two replicates were excluded from the following integrative processing.

For each replicate, the ratio of the post-trial filtration (or respiration) and the main-trial baseline filtration (or respiration) rate expressed as a fraction of 100 are provided as estimates of cumulative random effects, estimating how big the random effect is compared to the baseline response signal (Supplementary Information Table S3). A negative (or positive) effect means that non–filter-feeder factors might have led to a higher (or lower) food or dissolved oxygen measurements by $Sensor_{Sn}$ compared to $Sensor_C$ during the post-trial. The values indicate how much the filtration (or respiration) might have been under- or overestimated especially for data points recorded closer to the end of the main-trial period. The absolute value of average post-trial filtration rate was 0.1 mL min^{-1} that could be expressed as $\sim$ 0.2% with reference to the baseline rate. The remnants of mussels and the resulting microbial activity contributed to post-trial respiration rates, which was on average 0.016 $\mu molO_2$ min^{-1} (i.e., $\sim$ 7% of the mussels' mean baseline respiration). While the random effects cannot be corrected, their recognition can help the user to better interpret the results and decide if data of a replicate must be removed from the analysis due to large drifts.

The rates of scope for growth of the studied mussels, estimated based on calculated filtration rates at (hypothetical) concentrations of 1000 and 4000 cells mL^{-1}, are presented in Supplementary Information Fig. S9. It should be noted that our estimation of hypothetical SFG simplistically assumes that the respiration rate is independent of the ambient food concentration (not considering respiratory costs of the feeding at

different food levels; Secor 2009). Future users can also estimate "SFG at the experimental food regime" based on real-time feeding and respiration rates (plots not presented here). Notably, both experimental and hypothetical SFGs neglect that AE may vary when environmental conditions change, especially in relation to organic content of food and ingestion rate (Hawkins et al. 1996).

Temporal variation in rates of filtration and respiration averaged over pooled replicated data of the mussel-trials are presented in Fig. 5. The mean rates of filtration decreased with warming (Fig. 5a). The maximum tolerated temperature, at which a steep drop in average filtration rate could be observed, was $\sim 24^{\circ}$C during the warming phase. During the subsequent cooling phase, mussels started increasing their filtration at ~ 27–28°C; however, only to a maximum level of $\sim 50\%$ of the initial rate (Fig. 5a). The mean respiration rate started to decline during the warming phase at $\sim 24^{\circ}$C, down to half of the initial values, and then started to increase again during the subsequent cooling phase at $\sim 30^{\circ}$C, and finally reached the initial respiration rate (Fig. 5b). Variance (interindividual variability) was larger for the respiration-depression response than for the filtration shutdown.

The ambient food concentration and feeding rate of the study organisms over an experiment would be of interest to those investigating energetic costs of feeding or specific dynamic action (refer to Secor 2009). Considering the study question and the optimal filtration rates of the study specimens, one can regulate the food-tank concentration and the pumping rates to generate any ambient food concentrations of interest. Our studied mussels were large and their filtration activity on average decreased their ambient food concentration from ~ 3800 to 800 cells mL^{-1} over the period preceding the filtration shutdown (Supplementary Information Fig. S10a). Concentrations < 1000 cells mL^{-1} can be considered as marginal to suboptimal food levels for the filtration activity of *Mytilus* spp. (Riisgård et al. 2013); therefore, our studied mussels were probably food limited over that few-hour period. Mussels' respiration rates induced on maximum $\sim 10\%$ air-saturation decrease in dissolved oxygen (Supplementary Information Fig. S10b). The outflowing water oxygen levels remained above 80% saturation.

We compared our estimates of the baseline mean filtration and respiration rates of *Mytilus* specimens with the predictions based on previously published literature functions (Hamburger et al. 1983; Pleissner et al. 2013; more detailed description in Supplementary Information Text S5). The predicted rates of length-specific filtration and weight-specific respiration for *Mytilus* are 1.85 ($mL\ mm^{-1}\ min^{-1}$) and 0.41 ($\mu molO_2\ g^{-1}\ h^{-1}$). Our average baseline estimates were ~ 1.3 and 0.4, respectively (Fig. 5a,b), showing that our estimates are in line with the expectations.

Thermal variation in filtration and respiration rates in the warming and cooling phases of the mussel trails was described by generalized additive models (Fig. 6). Differences of the thermal response curves between the warming and cooling phases indicate time-dependent effects (i.e., in general, changes in the instant rate of thermal response over time due to alteration of the functional context by, for example, acclimatization, stress, and damage; Kingsolver et al. 2015).

Challenges and solutions provided by FOFS and the suggested data processing

In FOFS, we successfully used submersible fluorometers that are more affordable and easier to handle due to their small size compared to previously applied laboratory fluorometers (Haure et al. 2003; Pleissner et al. 2013). We provide the procedure for temperature correction and unit conversion of Chlorophyll data, which was successfully tested in the demonstration experiment. The Python scripts explicitly facilitate all steps of data processing, making our method more understandable and adaptable for future studies. It applies a robust modeling technique for denoising measurements. It includes the dampening-effect correction which can be applied to data obtained through similar flow-through setups (including aquarium or mesocosm-based systems) in which the sensors are inevitably positioned in a series of chambers of different sizes. The three-stage design of experimental trials enables estimation of cumulated random effects (as a measure of the temporal precision of measurements) soon after the end of a trial, allowing the users to exchange malfunctioning sensors in time and to better interpret the observed patterns of temporal variation in responses.

Other technical issues include the bubble formation in tubing and chambers and inherent differences between sensor readouts. These are explained and resolved in our method.

Limitations and potential solutions

Respiration rates recorded using FOFS represent the energy consumption rate by aerobic metabolism (Widdows and Hawkins 1989). To measure the rate of anaerobic metabolism, which might be especially important when filter-feeders experience phases of (thermally induced) metabolic depression (valve closure), a direct calorimetry method would have to be applied (Guppy and Withers 1999; Regan et al. 2013; Nelson 2016). Another limitation of FOFS is the lack of automated control over the ambient food level, which can change under the influence of any filter-feeders' filtration activity throughout an experiment (e.g., thermal shutdown of filtration). By developing a feedback loop connecting Cyclops fluorometers and Pump2 through their software interfaces in the present setup, it should be possible to upgrade the setup to a system allowing automated control of ambient food concentrations.

Biofilm or bio-deposit accumulation may limit the time window of continuous recording of respiration in FOFS experiments. After our 1.5-d-long trials, the respiration from the remnants of mussels and biofilms was, on average, ca. 7% of the mussels' mean baseline respiration (for mussels with ca. 4 cm shell length). To keep the error caused by microbial

respiration minimal, especially during longer term trials, one must stop the trial for a few minutes, for example, once a day, clean the incubation (Plexi-glass) chambers using deionized water and soft brush, and then continue the trial.

Significance, directions, and possible advancements of the method

The decadal to centennial patterns of thermal changes in shallow-water marine habitats can be decomposed into (1) long-term trends, (2) mid- and short-term (annual to daily) systematic fluctuations, and (3) stochastic fluctuations of various durations (minutes and hours to months) (Lima and Wethey 2012). Empirical studies recently inferred that, because of acclimatization and other time-dependent effects (e.g., physiological stress or damage), consequences of short-term environmental fluctuations on the ecological performance might differ from mathematical predictions based on performance curves empirically established under static treatment conditions (Niehaus et al. 2012; Kingsolver et al. 2015; Koussoroplis et al. 2017). Advancement in empirical methods is thus urgently needed to enable the description of the underlying causes of discrepancies between the predicted and observed effects of environmental fluctuations. FOFS practically provides a tool for researchers exposing organisms to environmental variability for some weeks or months, to relate the observed long-term integrated performance responses to short-term energy budget responses and explain their findings with the potential to generalize patterns. This procedure may improve the description of stress-response relationships and detection of species' tolerance limits.

The method can be used to provide more accurate data needed for parametrizing theoretical mechanistic models such as SFG (Winberg 1960) and dynamic energy budget models (Kooijman 2010). Besides, it will allow researchers to investigate interindividual variability in energetics responses of filter-feeders to temperature, mechanistically explaining intraspecies variability in growth, reproduction, and survival (Fuentes-Santos et al. 2018).

We tested the setup to describe mussels' responses to a scenario of daily thermal fluctuations. The setup with the attributes described here can be used in more extended trials (~ 7–10 d compared to 2 d currently), and to investigate responses of many other filter-feeding taxa. Also, this setup might be used to explain physiological responses of organisms (from online recordings) with data retrieved in longer term experiments (Pansch and Hiebenthal 2019; Morón Lugo et al. 2020). With minor modifications in chamber characteristics and flow-rates, the setup can be applied to studies of small- to large-sized filter-feeders, and may be extended to small communities of in- and epi-faunal suspension feeders. In that line, the setup can also be applied to test the response of systems of closely interacting species such as the filter-feeder-predator and filter-feeder-endoparasite systems to environmental variability (Stier et al. 2015). In principle, many drivers (e.g., temperature, oxygen, food, salinity, pH, and biological cues such as predator cues) can be manipulated in the setup, while respiration and filtration are constantly monitored. Therefore, we infer that the method can be adapted for multifactorial exploration of filter-feeders' ecophysiology.

Conclusions

We described and successfully demonstrated the functionality of a method, including the experimental setup (FOFS), design, and data processing protocols, enabling researchers to monitor energy budget responses including filtration and metabolic activities of benthic filter-feeders in response to fine-tuned environmental variability. Importantly, the method can be adapted to study multifactorial ecophysiology of shallow-water marine filter-feeders, shedding light onto species responses to environmental changes occurring within timescales of minutes or hours especially during daily cycles or extreme events such as marine heatwaves or hypoxic upwelling. This method can be applied by researchers exposing organisms to environmental variability for some weeks or months, to describe the observed integrated impacts of variability on the performance through energy budget responses to short-term environmental changes. In general, the method, therefore, allows a more mechanistic description of stress-response relationships and species' tolerance limits which are required for enhancing our understanding of filter feeders' performance responses to climate change.

Data availability statement

The data supporting the results of the demonstration experiment are archived in PANGEA (https://doi.org/10.1594/PANGAEA.919682).

References

Bayne, B. 2017. Biology of oysters, 1st Edition. Academic Press.

Boyd, P. W., C. E. Cornwall, and A. Davison. 2016. Biological responses to environmental heterogeneity under future ocean conditions. **22**: 2633–2650. doi:10.1111/gcb.13287

Burge, C. A., C. J. Closek, C. S. Friedman, M. L. Groner, C. M. Jenkins, A. Shore-Maggio, and J. E. Welsh. 2016. The use of filter-feeders to manage disease in a changing world. Integr. Comp. Biol. **56**: 573–587. doi:10.1093/icb/icw048

Campbell, S., and R. Haberman. 2008. Introduction to differential equations with dynamical systems. Princeton Univ. Press.

Clausen, I., and H. U. Riisgård. 1996. Growth, filtration and respiration in the mussel *Mytilus edulis*: No evidence for physiological regulation of the filter-pump to nutritional needs. Mar. Ecol. Prog. Ser. **141**: 37–45. doi:10.3354/meps14103

Dame, R. F., D. Bushek, and T. C. Prins. 2001. Benthic suspension feeders as determinants of ecosystem structure and

function in shallow coastal waters, p. 11–37.*In* K. Reise [ed.], Ecological comparisons of sedimentary shores. Ecological studies (analysis and synthesis). Springer. doi:10.1007/978-3-642-56557-1_2

Filgueira, R., U. Labarta, and M. J. Fernandez-Reiriz. 2006. Flow-through chamber method for clearance rate measurements in bivalves: Design and validation of individual chambers and mesocosm. Limnol. Oceanogr.: Methods **4**: 284–292. doi:10.4319/lom.2006.4.284

Fuentes-Santos, I., U. Labarta, and M. J. Fernández-Reiriz. 2018. Characterizing individual variability in mussel (*Mytilus galloprovincialis*) growth and testing its physiological drivers using functional data analysis. PLoS One **13**: 1–13. doi:10.1371/journal.pone.0205981

Gili, J. M., and R. Coma. 1998. Benthic suspension feeders: Their paramount role in littoral marine food webs. Trends Ecol. Evol. **13**: 316–321. doi:10.1016/S0169-5347(98)01365-2

Guppy, M., and P. Withers. 1999. Metabolic depression in animals: Physiological perspectives and biochemical generalizations. Biol. Rev. **74**: 1–40. doi:10.1111/j.1469-185X.1999.tb00180.x

Hamburger, K., F. Mohlenberg, A. Randlov, and H. U. Riisgård. 1983. Marine size, oxygen consumption and growth in the mussel *Mytilus edulis*. J. Mar. Biol. **75**: 303–306. doi:10.1007/BF00406016.

Haure, J., A. Huvet, H. Palvadeau, M. Nourry, C. Penisson, J. L. Y. Martin, and P. Boudry. 2003. Feeding and respiratory time activities in the cupped oysters *Crassostrea gigas*, *Crassostrea angulata* and their hybrids. Aquaculture **218**: 539–551. doi:10.1016/S0044-8486(02)00493-3

Hawkins, A. J. S., R. F. M. Smith, B. L. Bayne, and M. Héral. 1996. Novel observations underlying the fast growth of suspension-feeding shellfish in turbid environments: *Mytilus edulis*. Mar. Ecol. Prog. Ser. **131**: 179–190. doi:10.3354/meps131179

Hippke, M., T. J. David, G. D. Mulders, and R. Heller. 2019. Wōtan: Comprehensive time-series detrending in Python. Astron. J. **158**: 143. doi:10.3847/1538-3881/ab3984

Kingsolver, J. G., J. K. Higgins, and K. E. Augustine. 2015. Fluctuating temperatures and ectotherm growth: Distinguishing non-linear and time-dependent effects. J. Exp. Biol. **218**: 2218–2225. doi:10.1242/jeb.12073

Kiørboe, T., F. Mshlenberg, and K. Hamburgefl. 1985. Bioenergetics of the planktonic copepod *Acatia tonsa*: Relation between feeding, egg production and respiration, and composition of specific dynamic action. Mar. Ecol. **26**: 85–97. doi:10.3354/MEPS026085

Kittner, C., and H. U. Riisgård. 2005. Effect of temperature on filtration rate in the mussel *Mytilus edulis*: No evidence for temperature compensation. **305**: 147–152. doi:10.3354/meps305147.

Kooijman, S. A. L. M. 2010. Dynamic energy budget theory for metabolic organization, 3rd Edition. Cambridge Univ. Press. doi:10.1098/rstb.2010.0167

Koussoroplis, A. M., S. Pincebourde, and A. Wacker. 2017. Understanding and predicting physiological performance of organisms in fluctuating and multifactorial environments. Ecol. Monogr. **87**: 178–197. doi:10.1002/ecm.1247

Larsen, P. S., and H. U. Riisgård. 2011. Validation of the flow-through chamber (FTC) and steady-state (SS) methods for clearance rate measurements in filter-feeders. Biol. Open **1**: 6–11. doi:10.1242/bio.2011011

Lima, F. P., and D. S. Wethey. 2012. Three decades of high-resolution coastal sea surface temperatures reveal more than warming. Nat. Commun. **3**: 1–13. doi:10.1038/ncomms171

Morón Lugo, S. C., M. Baumeister, O. M. Nour, F. Wolf, M. Stumpp, and C. Pansch. 2020. Warming and temperature variability determine the performance of two invertebrate predators. Sci. Rep. **10**: 1–14. doi:10.1038/s41598-020-63679-0

Nelson, J. A. 2016. Oxygen consumption rate v. rate of energy utilization of fishes: A comparison and brief history of the two measurements. J. Fish Biol. **88**: 10–25. doi:10.1111/jfb.12824

Niehaus, A. C., M. J. Angilletta, M. W. Sears, C. E. Franklin, and R. S. Wilson. 2012. Predicting the physiological performance of ectotherms in fluctuating thermal environments. J. Exp. Biol. **215**: 694–701. doi:10.1242/jeb.05803

Pansch, C., and C. Hiebenthal. 2019. A new mesocosm system to study the effects of environmental variability on marine species and communities. Limnol. Oceanogr.: Methods **17**: 145–162. doi:10.1002/lom3.10306

Pleissner, D., K. Lundgreen, F. Lüskow, and H. U. Riisgård. 2013. Fluorometer controlled apparatus designed for long-duration algal-feeding experiments and environmental effect studies with mussels. J. Mar. Biol. **2013**: 401961. doi:10.1155/2013/401961.

PreSens. 2004. OXY-4 4-channel Fiber-Optic Oxygen Meter: Instruction manual.

PreSens. 2017. Oxygen Sensor Spots PSt3/PSt6: Instruction manual.

Przeslawski, R., S. Ahyong, M. Byrne, G. Wörheide, and P. Hutchings. 2008. Beyond corals and fish: The effects of climate change on noncoral benthic invertebrates of tropical reefs. Glob. Chang. Biol. **14**: 2773–2795. doi:10.1111/j.1365-2486.2008.01693

Regan, M. D., J. M. Gosline, and J. G. Richards. 2013. A simple and affordable calorespirometer for assessing the metabolic rates of fishes. J. Exp. Biol. **216**: 4507–4513. doi:10.1242/jeb.093500

Riisgård, H. 2001. On measurement of filtration rate in filter-feeders - the stony road to reliable data: Review and interpretation. Mar. Ecol. Prog. Ser. **211**: 275–291. doi:10.3354/meps211275

Riisgård, H. U., D. Pleissner, K. Lundgreen, and P. S. Larsen. 2013. Growth of mussels *Mytilus edulis* at algal (*Rhodomonas salina*) concentrations below and above saturation levels

for reduced filtration rate. Mar. Biol. Res. **9**: 1005–1017. doi:10.1080/17451000.2012.74254

Riisgård, H. U., J. Lassen, and C. Kittner. 2006. Valve-gape response times in mussels (*Mytilus edulis*) - effects of laboratory preceding-feeding conditions and *in situ* tidally induced variation in phytoplankton biomass. J. Shellfish. Res. **25**: 901–911. doi:10.2983/0730-8000(2006)25

Sanders, T., L. Schmittmann, J. C. Nascimento-Schulze, and F. Melzner. 2018. High calcification costs limit mussel growth at low salinity. Front. Mar. Sci. **5**: 1–9. doi:10.3389/fmars.2018.0035

Secor, S. M. 2009. Specific dynamic action: A review of the postprandial metabolic response. J. Comp. Physiol. B Biochem. Syst. Environ. Physiol. **179**: 1–56. doi:10.1007/s00360-008-0283-7

Servén, D., and C. Brummitt. 2018. pyGAM: Generalized additive models in Python. Zenodo. doi:10.5281/zenodo.1208723

Stier, T., J. Drent, and D. W. Thieltges. 2015. Trematode infections reduce clearance rates and condition in blue mussels *Mytilus edulis*. Mar. Ecol. Prog. Ser. **529**: 137–144. https://doi.org/10.3354/meps11250

Tang, B., and H. U. Riisgård. 2016. Physiological regulation of valve-opening degree enables mussels *Mytilus edulis* to overcome starvation periods by reducing the oxygen uptake. Open. J. Mar. Sci. **6**: 341–352. doi:10.4236/ojms.2016.63029

Turner Designs. Turner Designs; 2020. Cyclops submersible sensors: User's manual.

Vajedsamiei, J., F. Melzner, M. Raatz, R. Kiko, M. Khosravi, and C. Pansch. 2020. Exemplary FOFS output data of experiments on simultaneous recording of filtration and respiration in marine organisms. doi:10.1594/PANGAEA.919682

van der Schatte Olivier, A., L. Jones, L. Le Vay, M. Christie, J. Wilson, and S. K. Malham. 2018. A global review of the ecosystem services provided by filter-feeder aquaculture. Rev. Aquac. **12**: 1–23. doi:10.1111/raq.12301

Wahl, M., and others. 2015. A mesocosm concept for the simulation of near-natural shallow underwater climates: The Kiel Outdoor Benthocosms (KOB). Limnol. Oceanogr.: Methods **13**: 651–663. doi:10.1002/lom3.10055

Wahl, M., V. Saderne, and Y. Sawall. 2016. How good are we at assessing the impact of ocean acidification in coastal systems? Limitations, omissions and strengths of commonly used experimental approaches with special emphasis on the neglected role of fluctuations. Mar. Freshw. Res. **67**: 25–36. doi:10.1071/MF14154

Widdows, J. 1973. The effects of temperature on the metabolism and activity of *Mytilus edulis*. Net. J. Sea. Res. **398**: 387–398. doi:10.1016/0077-7579(73)90060-4.

Widdows, J. 1976. Physiological adaptation of *Mytilus edulis* to cyclic temperatures. J. Comp. Physiol. **105**: 115–128. doi:10.1007/BF0069111

Widdows, J., and A. J. S. Hawkins. 1989. Partitioning of rate of heat dissipation by *Mytilus edulis* into maintenance, feeding, and growth components. Physiol. Zool. **62**: 764–784.

Widdows, J., and B. L. Bayne. 1971. Temperature acclimation of *Mytilus edulis* with reference to its energy budget. J. Mar. Biol. Assoc. **51**: 827–843. doi:10.1017/S0025315400018002

Widdows, J., M. D. Brinsley, P. N. Salkeld, and M. Elliott. 1998. Use of annular flumes to determine the influence of current velocity and filter-feeders on material flux at the sediment-water interface. Estuaries **21**: 552–559. doi:10.2307/135329

Winberg, G. G. 1960. Rate of metabolism and food requirements of fishes. *In* F. E. J. Fry and W. E. Ricker [eds.], Translation Series No. 194. Fisheries Research Board of Canada.

Wood, S. N. 2017. Generalized additive models: An introduction with R, 2nd Edition. Chapman & Hall/CRC.

Acknowledgments

The authors would like to acknowledge Ulrike Panknin for providing the *Rhodomonas* culture and technical assistance. We also thank Dakeishla Mary Diaz Morales for her comments on the final manuscript and Prof. Martin Wahl for his supports throughout this project. This work and JV were funded through the Deutsche Forschungsgemeinschaft (DFG) project: The neglected role of environmental fluctuations as modulator of stress and driver of rapid evolution (Grant Number: PA 2643/2/348431475) and through GEOMAR. The project was supported by the Cluster of Excellence "The Future Ocean," funded within the framework of the Excellence Initiative by the DFG on behalf of the German federal and state governments. CP was funded by the postdoc program of the Helmholtz-Gemeinschaft Deutscher Forschungszentren and by GEOMAR. RK was supported by the collaborative research center 754 "Climate-Biogeochemistry Interactions in the Tropical Ocean" (www.sfb754.de) which was supported by the DFG. RK also acknowledges support from the Make Our Planet Great Again program of the French National Research Agency within the Programme d'Investissements d'Avenir; reference ANR-19-MPGA-0012. MK was funded through the PhD program of "studienstiftung des deutschen volkes". Open Access funding enabled and organized by ProjektDEAL.

Conflict of Interest

None declared.

Submitted 20 March 2020
Revised 26 August 2020
Accepted 24 December 2020

Associate editor: George Waldbusser